Spectral-Energy Trade-Offs in Memristor Programming Using Generalized Gaussian Voltage Pulses

E. Miranda, *Senior Member, IEEE*, E. Piros, T. Kim, P. Schreyer, J. Gehrunger, T. Oster, J. Suñé, *Fellow, IEEE*, C. Hochberger, *Senior Member, IEEE*, and L. Alff, *Member, IEEE*

***Abstract*—This work investigates the spectral and energetic aspects of memristor programming using generalized Gaussian voltage pulses. Unlike conventional square or triangular waveforms, generalized Gaussian pulses enable precise control over both temporal shape and frequency content through a tunable shape parameter. By systematically varying the pulse's effective width and sharpness, we analyze the resulting current response and its dependence on the memristor's nonlinear and memory-driven dynamics. SPICE simulations reveal how pulse shaping directly affects the spectral distribution, instantaneous power consumption, total programming energy, and programming time. The results highlight key trade-offs among frequency-domain characteristics, pulse amplitude, and energy efficiency, providing practical design guidelines for energy-aware memristive programming. Controlling the frequency spectrum in memristive circuits is critical to preventing parasitic elements in wires and devices from introducing additional signal distortion, which could compromise the accuracy and reliability of in-memory operations. These findings have potential implications for low-power neuromorphic computing, analog signal modulation, and waveform-optimized memory architectures.**

***Index Terms*—Memristor, frequency, energy, power, SPICE.**

I. Introduction

MEMRISTORS are two-terminal devices that encode information in the form of an electrical resistance state that persists after the programming signal is removed. The key theoretical elements underlying memristor behavior were originally proposed by L. Chua in his seminal works on nonlinear circuit theory [1], [2], [3]. This tunable and nonvolatile property of memristors is a hallmark of ReRAMs technologies, enabling their integration into memory arrays and neuromorphic computing systems [4]. Among the different programming schemes, including constant voltage or current, ramps, and pulses, the pulse-based approach is the most widely adopted owing to its superior control and precision [5], [6]. While extensive research has explored how the polarity and duty cycle of programming pulses affect resistive switching behavior [7], the spectral implications of pulse shape, particularly rise and fall times, remain underexplored. In practical scenarios, idealized square pulses are unattainable, and real voltage transitions inherently introduce frequency components beyond the fundamental. In this study, we focus on bipolar-type memristors where resistive switching involves the formation and rupture of conductive filaments across the dielectric layer in a metal-insulator-metal structure [8], [9]. Although filament dynamics are governed by ion drift and vacancy migration under the influence of the electric field, the interplay between pulse shape and internal state evolution becomes relevant, particularly when sharp transitions are present. This aspect was partially explored in [10], but exclusively in the context of voltage ramps with different sweep rates. To investigate these effects in more detail, we use generalized Gaussian (*GGP*) voltage pulses to program the device, allowing systematic variation of effective pulse width, amplitude, and sharpness while maintaining control over spectral content [11]. The simulations are performed using the Dynamic Memdiode Model (DMM) implemented in the SPICE environment, more specifically in LTspice XVII [12]. A wide range of experimental data fittings supporting the DMM can be found in [13], [14], and [15]. The frequency response of memristors has also been thoroughly discussed in [16], [17], [18], [19], [20], and [21].

The aim of this study is to provide insights into how waveform design influences power consumption, programming energy, and programming time. In addition, effective control of the frequency spectrum in memristive circuits is crucial to minimize the impact of parasitic capacitances and inductances, which can introduce signal distortion and undermine the accuracy and reliability of in-memory computing operations [13], [22]. SPICE-based simulations are presented to quantify these trade-offs under generalized pulsed stimulation. For the sake of completeness, the model script used to perform the calculations is included in the Appendix. This work highlights a theoretical aspect of memristor programming that remains unexplored and requires technology-specific experimental validation, an issue of growing importance given the increasing focus on energy-efficient device operation.

Received 16 December 2025; revised 29 December 2025; accepted 2 January 2026. Date of publication 15 January 2026; date of current version 26 February 2026. This work was supported in part by Merck KgaA (Sustainability Hub), Darmstadt, Germany, the Ministerio de Ciencia e Innovación, Spain under Project PID2022-139586NB-C41 and in part by the TUDa Research Fellowship Programme, the HORIZON Chips-JU 101194172 NeAIxt Project and the Agencia Española de Investigación (AEI) under Project PCI2025-163216. The review of this letter was arranged by Editor S. Amoroso. *(Corresponding author: E. Miranda.)*

E. Miranda and J. Suñé are with the Departament d'Enginyeria Electrònica, Universitat Autònoma de Barcelona, 08193 Cerdanyola del Vallès, Spain (e-mail: enrique.miranda@uab.cat).

E. Piros, T. Kim, P. Schreyer, and L. Alff are with the Institute of Materials Science, Technische Universität Darmstadt, 64287 Darmstadt, Germany.

J. Gehrunger, T. Oster, and C. Hochberger are with the Department of Electrical and Information Engineering, Technische Universität Darmstadt, 64283 Darmstadt, Germany.

Digital Object Identifier 10.1109/LED.2026.3653257

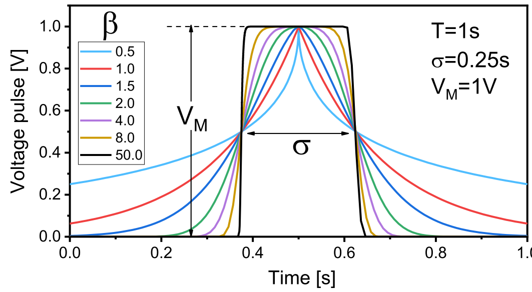

Fig. 1. Plot of generalized gaussian voltage pulses as a function of the shape parameter β. V_M is the amplitude and σ the width.

II. Method for Generating GGPs

A train of generalized Gaussian voltage pulses $V(t)$ can be constructed by composing a generalized Gaussian function with a linearly increasing ramped signal $x(t)$. This approach leverages the monotonicity of the ramp to map time directly into the argument of the Gaussian expression, effectively shaping the voltage waveform with precise temporal control. More concisely, we consider:

$$V(t) = V_M \exp\left\{-\ln(2)\left[\frac{2|x(t)|}{\sigma}\right]^{\beta}\right\} \tag{1}$$

with

$$x(t) = t - T\left[F\left(\frac{t}{T}\right) + \frac{1}{2}\right] \tag{2}$$

where t is the time, V_M the voltage pulse amplitude, β the shape parameter, σ the pulse full width at half maximum (FWHM), T the signal period, and F the floor function. For $\beta = 2$, (1) reduces to the well-known Gaussian pulse, if $\beta < 2$, the family of curves produces heavier tails than the Gaussian case ($\beta = 1$ corresponds to a Laplace, *i.e.* spike-like pulse). For $\beta > 2$, the pulse becomes increasingly sharp and localized, approaching a square pulse as $\beta \to \infty$ (see Fig. 1). Note that the compositional method proposed here is not limited to Gaussian functions; it can be generalized to synthesize a wide variety of waveforms by applying different mathematical envelopes (e.g., Lorentzian, double-exponential, sinusoidal windows) to a ramp function. In this formulation, the ramp acts as a temporal carrier, while the envelope defines the final waveform shape. This approach is particularly useful in circuit-simulation environments such as SPICE, where constructing complex time-domain signals from primitive elements (ramps and mathematical expressions) provides flexible control without relying on predefined waveform sources. Practical implementations of Gaussian voltage-pulse generators can be found in [23], [24], [25], [26], and [27].

III. Frequency Effects on the I-V Characteristic

In the DMM [14], the current-voltage (*I-V*) characteristic and internal memory state $0 \le g \le 1$ of a bipolar-type memristor are described by the following set of coupled nonlinear equations:

$$I(V) = \left[\left(I_{on} - I_{off}\right) g + I_{off}\right] \sinh\left[\alpha V_B\right] \tag{3}$$

$$\frac{dg}{dt} = \frac{1}{T_0}\left[(1-g) H(V_B) + gH(-V_B)\right] \sinh\left(\frac{V_B}{V_0}\right) \tag{4}$$

where $V_B = V\text{-}IR$ is the applied voltage corrected by the snapback series resistance R. α, T_0, and V_0 are fitting constants,

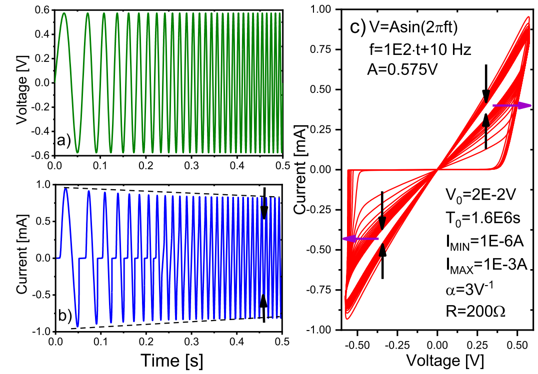

Fig. 2. a) Chirp sinusoidal voltage signal. b) Current-time characteristic. Dashed lines indicate the reduction of the current window. c) Shrink of the *I*-V loop (black arrows) and shift of the set and reset voltages (violet arrows) as the signal frequency increases.

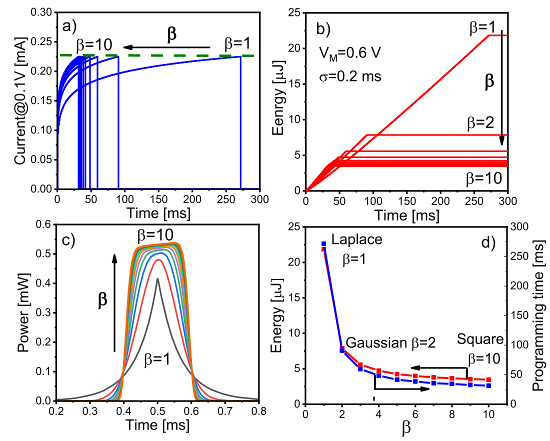

Fig. 3. a) Evolution of the read current (*I*@0.1V) for different β values. The current drop indicates the target state (g_f = 0.75) was reached. b) Consumed energy as a function of time. c) Dissipated power for a single isolated pulse. d) Summary plot for the energy and programming time as a function of β.

and I_{on} and I_{off} are calibration factors for the maximum and minimum currents, respectively. For simplicity, (4) assumes symmetric set ($V > 0$) and reset ($V < 0$) characteristic switching times. The hyperbolic function in (4) represents the exponential drift times of oxygen vacancies and metal ions within the dielectric film [28], incorporating a correction to ensure detailed balance at zero voltage. $H(x)$ is the Heaviside function. Figure 2 illustrates the effects of a chirp sinusoidal signal on the *I-V* curve. As the signal frequency increases (Fig. 2a), the effective set and reset voltages also increase, leading to switching suppression (Fig. 2b) and a shrinking hysteresis loop (Fig. 2c), in agreement with Chua's theory [3], [29]. The magnitude of this effect depends on the values of the moving set and reset voltages relative to the amplitude of the applied signal. This clearly indicates that higher frequencies, when amplitude-limited, do not provide sufficient energy to induce switching, as experimentally demonstrated in [20] and [21].

IV. Effects of the Signal Shape

As shown in Section III, for a fixed amplitude, increasing the frequency reduces the effectiveness of the electrical stimulus in altering the memristor state. From a physical perspective, this behavior arises from the limited ability of vacancies or ions to follow the applied signal, as their motion

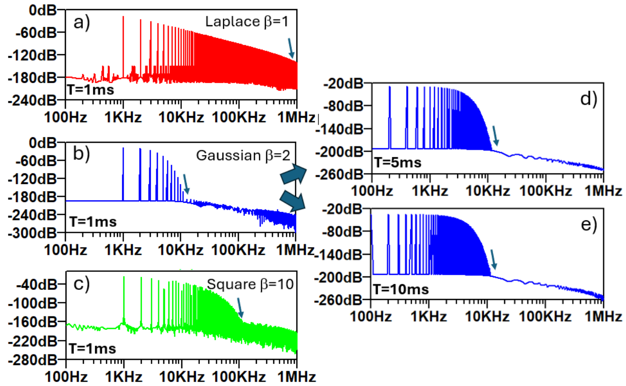

Fig. 4. Signal spectrum (Fast Fourier Transform, FFT) of the applied voltage $V(t)$ for selected values of β and period T. Panels a), b), and c) correspond to $\beta = 1$ (Laplace), $\beta = 2$ (Gaussian), and $\beta = 10$ (square), respectively, all evaluated with $T = 1$ ms. Panels d) and e) were calculated for $\beta = 2$ (Gaussian) using different periods, 5 ms and 10 ms, respectively. Note the attenuation of the spectral amplitude at specific cutoff frequencies (black arrows).

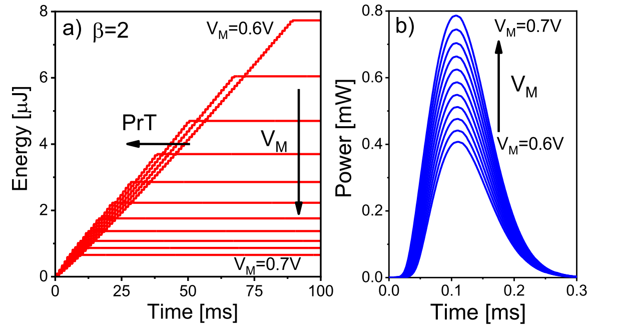

Fig. 5. a) Consumed energy as a function of time for gaussian pulses ($\beta = 2$) with different amplitude. b) Power dissipation for a single isolated pulse.

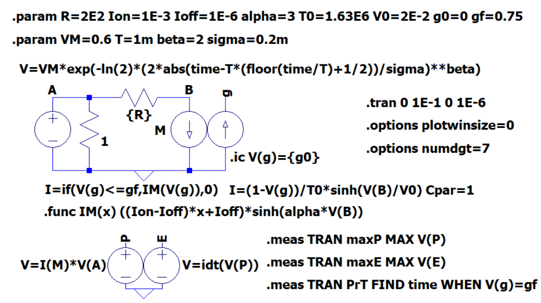

Fig. 6. LTspice schematic used for the computations presented in this work. For simplicity, only the set process is considered here.

requires longer timescales to produce structural changes [18]. This naturally raises the question of how the device response evolves when the fundamental frequency of the signal is kept constant but the spectral content of the programming pulse is systematically varied, which we accomplish by reshaping the pulse. To address this, we analyze the dissipated power ($P = IV$), the energy consumption ($E = \int P(t)dt$), and the programming time PrT (time required to reach a target memory state, *i.e.* $time@g_f$). Fig. 3 illustrates model results keeping V_M and σ constant while varying the pulse shape through the parameter β. Fig. 3a shows the evolution of the read current (I@0.1V) for different values of β. As expected, as β increases, the final state g_f is reached earlier. Fig. 3b also shows that programming with square pulses ($\beta = 10$) requires less energy than with Laplace pulses ($\beta = 1$). However, the slope of the curves indicates that programming can be achieved with lower peak power at smaller β values. This behavior is consistent with the results in Fig. 3c for a single isolated pulse. Fig. 3d summarizes E and PrT as functions of β. For *GGP*s of different shapes, E and PrT are directly related, but reducing both comes at the cost of increased instantaneous peak power, which may lead to enhanced Joule heating. The model script used to obtain these results is provided in the Appendix of this work. For a more realistic approach, variability can be incorporated into the definition of the model parameters using random distributions as reported in [30].

V. Role of the Signal Frequency Content

Let us analyze in more detail the implications of a given pulse shape. As shown in Fig. 4, the frequency-domain behavior of *GGP*s strongly depends on β: not only do lower β values produce pulses with broad spectra and greater high-frequency content (Fig. 4a), but higher β values also exhibit a similar trend (Fig. 4c). Notably, $\beta = 2$ corresponds to the lowest overall frequency content (Fig. 4b), making it the ideal value for minimizing any effects arising from parasitic components in memristor-based circuits [13]. It is worth noting that increasing the signal period T reduces the spacing between the individual frequency components (Figs. 4d,e), while the highest frequency component (cutoff frequency) remains nearly unchanged. This behavior directly follows from the time-frequency uncertainty principle [31]. As expected, T does not affect the total energy consumption or the maximum dissipated power, but it does determine the programming time (not shown here).

To exploit the fact that a train of standard Gaussian pulses ($\beta = 2$) exhibits reduced spectral content (the Fourier transform of a Gaussian signal is another Gaussian signal), their amplitude can be increased to shorten the overall programming time (Fig. 5a). Because the spectral profile of the input signal remains unchanged, this strategy enables faster programming and lower energy consumption without introducing additional high-frequency components. The trade-off, as before, is an increase in instantaneous power dissipation (Fig. 5b). A comprehensive analysis must also account for the harmonic distortion generated by the nonlinear device; however, this effect is specific to the circuit under consideration [32].

Appendix

The LTspice schematic used to perform the computations reported in this work is shown in Fig. 6. The model parameters are defined in the main text. (1) and (2) are combined into a single expression for the applied signal. A shunt resistance with a value of 1 Ω is used to redirect the electron current flowing through the memristor (IM) once the target memory state g_f is reached (g_0 being the initial memory value). A capacitor with Cpar= 1 F is employed to integrate the differential equation (4). Only potentiation is considered in this script. The *plotwinsize* and *numdgt* commands are optional directives that improve the computation of the signal spectrum (FFT operation in LTspice). The *idt* function represents the time integral. The *.meas* statements are post-processing directives used to calculate the maximum power, total energy, and programming time.

References

[1] L. Chua, "Memristor—The missing circuit element," *IEEE Trans. Circuit Theory*, vol. CT-18, no. 5, pp. 507–519, May 1971, doi: 10.1109/TCT.1971.1083337.

[2] L. O. Chua and S. Mo Kang, "Memristive devices and systems," *Proc. IEEE*, vol. 64, no. 2, pp. 209–223, 1976, doi: 10.1109/PROC.1976.10092.

[3] L. Chua, "Resistance switching memories are memristors," *Appl. Phys. A, Solids Surf.*, vol. 102, no. 4, pp. 765–783, Mar. 2011, doi: 10.1007/s00339-011-6264-9.

[4] F. Aguirre, A. Sebastian, M. Le Gallo, W. Song, T. Wang, J. J. Yang, W. Lu, M.-F. Chang, D. Ielmini, Y. Yang, A. Mehonic, A. Kenyon, M. A. Villena, J. B. Roldán, Y. Wu, H.-H. Hsu, N. Raghavan, J. Suñé, E. Miranda, A. Eltawil, G. Setti, K. Smagulova, K. N. Salama, O. Krestinskaya, X. Yan, K.-W. Ang, S. Jain, S. Li, O. Alharbi, S. Pazos, and M. Lanza, "Hardware implementation of memristor-based artificial neural networks," *Nature Commun.*, vol. 15, no. 1, Mar. 2024, Art. no. 1974, doi: 10.1038/s41467-024-45670-9.

[5] V. Milo, A. Glukhov, E. Perez, C. Zambelli, N. Lepri, M. K. Mahadevaiah, E. P.-B. Quesada, P. Olivo, C. Wenger, and D. Ielmini, "Accurate program/verify schemes of resistive switching memory (RRAM) for in-memory neural network circuits," *IEEE Trans. Electron Devices*, vol. 68, no. 8, pp. 3832–3837, Aug. 2021, doi: 10.1109/TED.2021.3089995.

[6] W. Song, M. Rao, Y. Li, C. Li, Y. Zhuo, F. Cai, M. Wu, W. Yin, Z. Li, Q. Wei, S. Lee, H. Zhu, L. Gong, M. Barnell, Q. Wu, P. A. Beerel, M. S.-W. Chen, N. Ge, M. Hu, Q. Xia, and J. J. Yang, "Programming memristor arrays with arbitrarily high precision for analog computing," *Science*, vol. 383, no. 6685, pp. 903–910, Feb. 2024, doi: 10.1126/science.adi9405.

[7] S. Brivio, S. Spiga, and D. Ielmini, "HfO_2-based resistive switching memory devices for neuromorphic computing," *Neuromorphic Comput. Eng.*, vol. 2, no. 4, Dec. 2022, Art. no. 042001, doi: 10.1088/2634-4386/ac9012.

[8] A. Padovani, L. Larcher, O. Pirrotta, L. Vandelli, and G. Bersuker, "Microscopic modeling of HfOx RRAM operations: From forming to switching," *IEEE Trans. Electron Devices*, vol. 62, no. 6, pp. 1998–2006, Jun. 2015, doi: 10.1109/TED.2015.2418114.

[9] S. Petzold, E. Piros, R. Eilhardt, A. Zintler, T. Vogel, N. Kaiser, A. Radetinac, P. Komissinskiy, E. Jalaguier, E. Nolot, C. Charpin-Nicolle, C. Wenger, L. Molina-Luna, E. Miranda, and L. Alff, "Tailoring the switching dynamics in yttrium oxide-based RRAM devices by oxygen engineering: From digital to multi-level quantization toward analog switching," *Adv. Electron. Mater.*, vol. 6, no. 11, Nov. 2020, Art. no. 2000439, doi: 10.1002/aelm.202000439.

[10] E. Miranda, E. Piros, F. L. Aguirre, T. Kim, P. Schreyer, J. Gehrunger, T. Schwarz, T. Oster, K. Hofmann, J. Suñé, C. Hochberger, and L. Alff, "Analysis of the voltage ramp rate effects on the programming characteristics of bipolar-type memristive devices," *IEEE Trans. Nanotechnol.*, vol. 24, pp. 205–208, 2025, doi: 10.1109/TNANO.2025.3556856.

[11] S. Nadarajah, "A generalized normal distribution," *J. Appl. Statist.*, vol. 32, no. 7, pp. 685–694, Sep. 2005, doi: 10.1080/02664760500079464.

[12] *Analog Devices*. Accessed: Jan. 15, 2026. [Online]. Available: https://www.analog.com/en/resources/design-tools-and-calculators

[13] F. L. Aguirre, S. M. Pazos, F. Palumbo, J. Suñé, and E. Miranda, "Application of the quasi-static memdiode model in cross-point arrays for large dataset pattern recognition," *IEEE Access*, vol. 8, pp. 202174–202193, 2020, doi: 10.1109/ACCESS.2020.3035638.

[14] F. L. Aguirre, J. Suñé, and E. Miranda, "SPICE implementation of the dynamic memdiode model for bipolar resistive switching devices," *Micromachines*, vol. 13, no. 2, p. 330, Feb. 2022, doi: 10.3390/mi13020330.

[15] F. Aguirre, E. Piros, N. Kaiser, T. Vogel, S. Petzold, J. Gehrunger, T. Oster, K. Hofmann, C. Hochberger, J. Suñé, L. Alff, and E. Miranda, "Simulation of the effect of material properties on yttrium oxide memristor-based artificial neural networks," *APL Mach. Learn.*, vol. 1, no. 3, Sep. 2023, Art. no. 036104, doi: 10.1063/5.0143926.

[16] K. A. Campbell, K. T. Drake, and E. H. Barney Smith, "Pulse shape and timing dependence on the spike-timing dependent plasticity response of ion-conducting memristors as synapses," *Frontiers Bioeng. Biotechnol.*, vol. 4, Dec. 2016, Art. no. 97, doi: 10.3389/fbioe.2016.00097.

[17] M. Uddin, Md. B. Majumder, and G. S. Rose, "Robustness analysis of a memristive crossbar PUF against modeling attacks," *IEEE Trans. Nanotechnol.*, vol. 16, no. 3, pp. 396–405, May 2017, doi: 10.1109/TNANO.2017.2677882.

[18] M. Maestro-Izquierdo, M. B. Gonzalez, F. Campabadal, J. Suñé, and E. Miranda, "A new perspective towards the understanding of the frequency-dependent behavior of memristive devices," *IEEE Electron Device Lett.*, vol. 42, no. 4, pp. 565–568, Apr. 2021, doi: 10.1109/LED.2021.3063239.

[19] V. Ostrovskii, P. Fedoseev, Y. Bobrova, and D. Butusov, "Structural and parametric identification of knowm memristors," *Nanomaterials*, vol. 12, no. 1, p. 63, Dec. 2021, doi: 10.3390/nano12010063.

[20] H. García, G. Vinuesa, E. García-Ochoa, F. L. Aguirre, M. B. González, F. Jiménez-Molinos, F. Campabadal, J. B. Roldán, E. Miranda, S. Dueñas, and H. Castán, "Effects of the voltage ramp rate on the conduction characteristics of HfO_2-based resistive switching devices," *J. Phys. D, Appl. Phys.*, vol. 56, no. 36, Sep. 2023, Art. no. 365108, doi: 10.1088/1361-6463/acdae0.

[21] D. Maldonado, G. Vinuesa, S. Aldana, F. L. Aguirre, A. Cantudo, H. García, M. B. González, F. Jiménez-Molinos, F. Campabadal, E. Miranda, S. Dueñas, H. Castán, and J. B. Roldán, "A thorough investigation of the switching dynamics of TiN/Ti/10 nm-HfO_2/W resistive memories," *Mater. Sci. Semiconductor Process.*, vol. 169, Jan. 2024, Art. no. 107878, doi: 10.1016/j.mssp.2023.107878.

[22] S. A. Thomas, R. Sharma, and D. M. Das, "Analyzing the impact of parasitics on a CMOS-memristive crossbar neural network based on winner-take-all and Hebbian rule," *Memories-Mater., Devices, Circuits Syst.*, vol. 5, Oct. 2023, Art. no. 100081, doi: 10.1016/j.memori.2023.100081.

[23] V. Alimisis, M. Gourdouparis, G. Gennis, C. Dimas, and P. P. Sotiriadis, "Analog Gaussian function circuit: Architectures, operating principles and applications," *Electronics*, vol. 10, no. 20, p. 2530, Oct. 2021, doi: 10.3390/electronics10202530.

[24] C. R. Popa, "High-accuracy Gaussian function generator for neural networks," *Electronics*, vol. 12, no. 1, p. 24, Dec. 2022, doi: 10.3390/electronics12010024.

[25] A. I. Bautista-Castillo, J. M. Rocha-Perez, A. Diaz-Sanchez, J. Lemus-Lopez, and L. A. Sanchez-Gaspariano, "A CMOS Morlet wavelet generator," *Radioengineering*, vol. 26, no. 1, pp. 263–268, Apr. 2017, doi: 10.13164/re.2017.0263.

[26] S. M. Eisa, H. H. Issa, K. A. Shehata, and H. F. Ragai, "Design and analysis of a low power UWB pulse generators," *Int. J. Comput. Electr. Eng.*, vol. 6, no. 3, pp. 244–247, 2014, doi: 10.7763/ijcee.2014.v6.831.

[27] M. Blank, T. Glueck, A. Kugi, and H.-P. Kreuter, "EMI reduction for smart power switches by iterative tracking of a Gaussian-shape switching transition," in *Proc. Int. Exhib. Conf. Power Electron., Intell. Motion, Renew. Energy Energy Manage.*, May 2015, pp. 1–8.

[28] E. Miranda, E. Piros, F. L. Aguirre, T. Kim, P. Schreyer, J. Gehrunger, T. Schwarz, T. Oster, K. Hofmann, J. Suñé, C. Hochberger, and L. Alff, "The role of the programming trajectory in the power dissipation dynamics and energy consumption of memristive devices," *IEEE Electron Device Lett.*, vol. 45, no. 4, pp. 582–585, Apr. 2024, doi: 10.1109/LED.2024.3368146.

[29] S. P. Adhikari, M. P. Sah, H. Kim, and L. O. Chua, "Three fingerprints of memristor," *IEEE Trans. Circuits Syst. I, Reg. Papers*, vol. 60, no. 11, pp. 3008–3021, Nov. 2013, doi: 10.1109/TCSI.2013.2256171.

[30] J. B. Roldán, E. Miranda, D. Maldonado, A. Mikhaylov, N. V. Agudov, A. A. Dubkov, M. N. Koryazhkina, M. B. González, M. A. Villena, S. Poblador, M. Saludes-Tapia, R. Picos, F. Jiménez-Molinos, S. G. Stavrinides, E. Salvador, F. Alonso, F. Campabadal, B. Spagnolo, M. Lanza, and L. O. Chua, "Variability in resistive memories," *Adv. Int. Sys.*, vol. 5, no. 6, 2023, Art. no. 2200338, doi: 10.1002/aisy.202200338.

[31] C. Paul, *Introduction to Electromagnetic Compatibility*, 2nd ed., Hoboken, NJ, USA: Wiley, 2006.

[32] F. Yang, A. Serb, and T. Prodromakis, "Measured behaviour of a memristor-based tuneable instrumentation amplifier," *Electron. Lett.*, vol. 58, no. 15, pp. 570–572, Jul. 2022, doi: 10.1049/ell2.12520.